Experimental Demonstration of Dynamical Input Isolation in Nonadiabatically Modulated Photonic Cavities

Avik Dutt,[†] Momchil Minkov,[†] Qian Lin,[‡] Luqi Yuan,[†] David A. B. Miller,[†] and Shanhui Fan*,[†]

[†]Ginzton Laboratory and Department of Electrical Engineering, Stanford University, Stanford, California 94305, United States
[‡]Department of Applied Physics, Stanford University, 348 Via Pueblo, Stanford, California 94305, United States

ABSTRACT: Modulated optical cavities have been proposed and demonstrated for applications in communications, laser frequency stabilization, microwave-to-optical conversion, and frequency comb generation. However, most studies are restricted to the adiabatic regime, where either the maximum excursion of the modulation or the modulation frequency itself is below the line width of the cavity. Here, using a fiber ring resonator with an embedded electro-optic phase modulator, we investigate the nonadiabatic regime. By strongly driving the modulator at frequencies that are significantly smaller than the free spectral range of the ring resonator, but well beyond the line width of the resonator, we experimentally observe counterintuitive behavior predicted in a recent theoretical study by Minkov et al. (APL Photonics **2017**, 2, 076101), such as the complete suppression of drop-port transmission even when the input laser wavelength is on resonance with the optical cavity. This can be understood as dynamical isolation of the cavity from the input light. We also show qualitative differences in the steady-state responses of the system between the adiabatic and nonadiabatic limits. Our experiments probe a seldom explored regime of operation that is promising for applications in integrated photonic systems with current state-of-the-art technology.

KEYWORDS: optical resonators, periodically driven systems, electro-optic modulation, optical fibers, lithium niobate, dynamical decoupling, driven-dissipative systems, Floquet systems
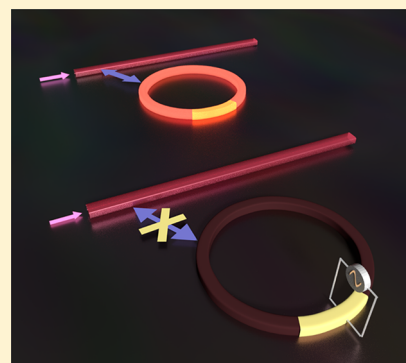
Dynamically modulated optical cavities are important for applications such as optical communications,[1−4] quantum state transfer between microwave and optical photons,[5,6] and signal processing.[3,7,8] They are a simple example of a class of driven-dissipative models which have been widely analyzed using Floquet techniques.[9−11] Specifically, ultracold atoms in periodically driven optical lattices have been used for realizing modulated intersite hoppings, synthetic gauge fields, and coherent destruction of tunneling.[12−16] In photonics, modulated ring resonators, where the refractive index of a portion of the ring is varied periodically in time, have been predominantly explored in two qualitatively different regimes. In the first regime, the modulation is at or near the free spectral range (FSR) of the cavity to couple multiple longitudinal frequency modes. This regime finds use in active mode locking of ultrashort pulses,[17] generating frequency combs,[18−22] and in realizing synthetic frequency dimensions.[23−28] In the second regime, the modulation frequency is far below the FSR, and this finds applications in realizing efficient and compact electro-optic modulators (EOMs).[1,4,29−32] Here, a single-mode description of the cavity suffices. Previous work in this case has almost exclusively focused on the adiabatic regime, which includes the case where the modulation strength is sufficiently small, and the modulation frequency is less than the cavity line width. For a static resonator, the transport properties of light through a resonator are determined by the resonant frequency. In the adiabatic regime, the transport

properties of the resonators are determined by the instantaneous resonant frequency.

Recent theoretical work predicts that for the single-mode case, but beyond the adiabatic regime, there exists interesting physics and counterintuitive effects.[33] In particular, the intracavity power in a dynamically modulated ring resonator can be completely suppressed even when the input laser is on resonance with the ring, as opposed to the static ring, where the intracavity power is maximized on resonance. Thus, a dynamical isolation of the cavity from the input laser can be achieved by operating in the nonadiabatic regime.[33,34] The related but different phenomena of dynamic localization and dynamical decoupling have been well known in electronic systems, in circuit quantum electrodynamics, and other quantum information contexts.[11,35−41]

In this paper we present an experimental exploration of such a dynamically modulated ring resonator in the nonadiabatic regime. Using a geometry consisting of a modulated fiber ring cavity coupled with two waveguides, we probe the nonadiabatic regime to demonstrate dynamical isolation and the suppression of drop-port transmission on resonance, based on the aforementioned analytical work.[33] Our experiments can have applications in using dynamic modulation for switching,
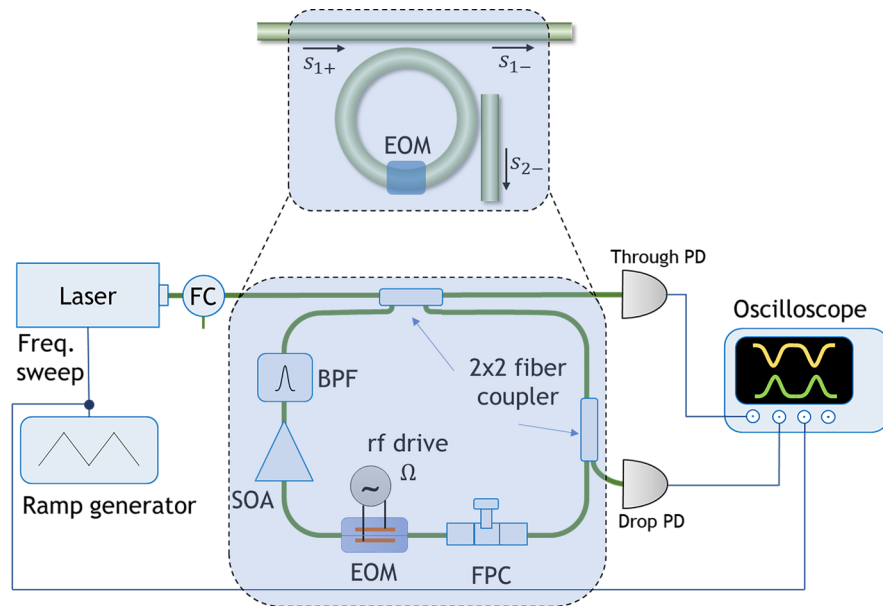
Figure 1. Experimental setup. The laser's frequency can be scanned by applying a ramp to its frequency sweep input. The rf drive's amplitude and frequency are chosen appropriately to probe either the nonadiabatic or the adiabatic regime. EOM: electro-optic modulator. FPC: fiber polarization controller. PD: photodiode. BPF: bandpass filter, 26 GHz bandwidth centered at 1542.14 nm. SOA: semiconductor optical amplifier. FC: fiber circulator.

optical signal processing, waveform synthesis, and frequency conversion of light.

■ THEORY

We start by briefly summarizing the relevant theoretical results in ref 33. For a ring cavity that is side coupled to two waveguides as shown in Figure 1(a), the coupled-mode equations for the mode amplitude α are[42,43]

$$\frac{d\alpha}{dt} = [i(\omega_0 + \omega(t)) - \gamma]\alpha + \sqrt{\gamma}s_{1+}$$

$$s_{1-} = -s_{1+} + \sqrt{\gamma}\alpha(t); \quad s_{2-} = \sqrt{\gamma}\alpha(t)$$

where s_{j+} and s_{j-} represent the input and output amplitudes in the j-th port, ($j = 1, 2$); $|\alpha|^2$ depicts the electromagnetic energy inside the cavity as carried by a circulating mode; $|s_{j\pm}|^2$ are the respective powers; and γ is the decay rate of the cavity into either of the waveguides. We assume that the through port ($j = 1$) and the drop port ($j = 2$) have the same decay rate γ and that the intrinsic loss in the ring can be neglected. ω_0 is the static resonance frequency of the cavity, and $\omega(t)$ is the time-dependent frequency modulation imparted by the electro-optic drive. The countercirculating mode of the resonator has been ignored in the above equations.

For a monochromatic input field $s_{1+} = p_0 \exp[i(\omega_0 + \Delta\omega)t]$ and a co-sinusoidal modulation of the resonant frequency $\omega(t) = A_0 \cos \Omega t$, it was shown that the steady-state solution for the drop-port output field s_{2-} is[33]

$$s_{2-}(t) = p_0 e^{i(\omega_0 + \Delta\omega)t} \sum_n s_n(\Delta\omega)e^{in\Omega t}$$

where

$$s_n(\Delta\omega) = -\sum_k J_{n+k}\left(\frac{A_0}{\Omega}\right)J_k\left(\frac{A_0}{\Omega}\right)\frac{\gamma}{ik\Omega - i\Delta\omega - \gamma} \quad (1)$$

The transmission at the drop port can be calculated from $T(t) = |s_{2-}|^2/p_0 = \sum_n T_n e^{in\Omega t}$, with $T_n = \sum_m s_m^* s_{n+m}$. Equation 1, which was derived in ref 33, is in agreement with the results in ref 44, but its novel consequences in the high-frequency nonadiabatic regime were first discussed in ref 33. Equation 1 was also recently derived in ref 45.

In the adiabatic limit predominantly studied in cavity-based modulators,[4] the transmission can be written as

$$T(t) = T(\omega(t)) = \left|\frac{\gamma}{i(\omega(t) - \Delta\omega) - \gamma}\right|^2 \quad (2)$$

This solution is valid for

$$\frac{A_0}{\Omega} \ll \left(\frac{\gamma}{\Omega}\right)^2 \quad (3)$$

which we call the adiabaticity condition. Since A_0/Ω was typically of order unity or less in nearly all previous studies of modulated cavities in the single-mode regime, it suffices to say that the adiabaticity is satisfied when the modulation frequency is much smaller than the line width of the cavity, or equivalently, the modulation period is much larger than the photon lifetime in the cavity. In this regime, the transmission shows a time variation on a time scale of the modulation frequency.

In the opposite regime, especially when $\gamma \ll \Omega$, the transmission becomes approximately independent of time.[33] In particular, significant transmission only occurs when $\Delta\omega \approx k\Omega$, with k being an integer, in which cases the transmission at every time t has the form

$$T(\Delta\omega \approx k\Omega) = J_k^2\left(\frac{A_0}{\Omega}\right)\left|\frac{\gamma}{i(\Delta\omega - k\Omega) - \gamma}\right|^2 \quad (4)$$

Thus, the transmission can be completely suppressed for zero laser-cavity detuning, i.e., $\Delta\omega = 0$, if the peak phase excursion of the modulation A_0/Ω is a zero of the Bessel function J_0.[33]

This is essentially a classical dynamical isolation effect, in which the effective amplitude of the input pump field is rescaled due to the modulation. For a more transparent explanation, one can use effective equations for the fields averaged over one modulation cycle, $T_M = 2\pi/\Omega$. Following the treatment of Salerno and Carusotto,[34] we define $\beta(t) = \alpha(t) \exp[(-i(\omega_0 + \Delta\omega)t - i\int_0^t \omega(t') \, dt']$. The effective equations for the fields then are

$$\frac{d\beta}{dt} = [i(\omega_0 + \Delta\omega) - \gamma]\beta + \sqrt{\gamma}\, s_{1+}^{eff}$$

where s_{1+}^{eff} is the rescaled pump amplitude or the effective averaged input field,

$$s_{1+}^{eff} \equiv \frac{p_0}{T_M} \int_0^{T_M} dt \; e^{-i\int_0^t \omega(t')dt'} = \frac{p_0}{T_M} \int_0^{T_M} dt \; e^{-i(A_0/\Omega)\sin\Omega t}$$

$$= p_0 J_0\!\left(\frac{A_0}{\Omega}\right)$$

This again shows the condition for dynamical isolation to be $J_0(A_0/\Omega) = 0$. This criterion should, however, be distinguished from dynamic localization (or decoupling), which applies in the case of coupled resonators or systems with two or more states and in which the rescaled quantity is the hopping rate between them. Indeed, note that the condition for dynamical isolation here is $J_0(A_0/\Omega) = 0$, while in the case of two resonators modulated off-phase, the condition for dynamic localization is $J_0(2A_0/\Omega) = 0$.[9,34,46] Note that this is strikingly different from both the static cavity, where the intracavity power and the drop-port transmission are maximum for zero detuning, and from the adiabatic regime, where the transmission is determined by the instantaneous frequency of the modulated cavity. In this high-frequency nonadiabatic regime, the transmission can be suppressed even though there are times when the instantaneous frequency of the cavity is on resonance with the incident wave. More generally, this suppression can be realized for a nonzero detuning that is an integer multiple of the modulation frequency ($\Delta\omega = k\Omega$) by choosing the modulation strength to be a zero of the kth order Bessel function J_k.

■ EXPERIMENTAL SETUP

We experimentally demonstrate the effect of dynamic isolation in a nonadiabatically modulated cavity[33] by incorporating an EOM into a fiber ring resonator, as shown in Figure 1. As discussed above, to reach the nonadiabatic regime the key is to modulate the cavity at frequencies Ω much higher than the cavity line width γ. Moreover, in order to be able to demonstrate the effect of dynamic isolation, the strength of the modulation A_0 needs to be comparable to the modulation frequency Ω. Thus, the experimental setup needs to simultaneously satisfy the following conditions: (i) low round-trip losses, which reduces γ, (ii) a large modulation frequency Ω, and (iii) a low half-wave voltage, V_π for the modulator, which is the voltage required to induce a phase shift of π. The last criterion ensures that a large modulation amplitude A_0 can be achieved for a reasonable voltage. We ensure low round-trip losses by introducing an optical amplifier to compensate for the insertion loss of intracavity components and connectors.[47] The cavity contains a fiber-coupled lithium niobate phase modulator with a moderately low V_π and a sufficiently large maximum modulation frequency of 2 GHz to enable us to reach the nonadiabatic regime and to achieve a

large modulation amplitude A_0. Note that such all-fiber configurations have been previously explored for realizing synthetic photonic lattices,[48] for generating frequency combs,[18−22] for demonstrating optical Ising machines,[49] and for producing nonclassical squeezed light.[50]

The detailed experimental setup is shown in Figure 1. A fiber ring resonator is built from commercially available off-the-shelf components. The ring is coupled to an input fiber through a 2 × 2, 99:1 fused fiber splitter. We excite the ring with a RIO Orion laser (grade 3, line width 2.8 kHz, center wavelength 1542.057 nm). The laser's frequency can be scanned over a 400 MHz range (∼3.2 pm in wavelength) by applying a voltage ramp to the frequency sweep input. A circulator was used before the fiber splitter to monitor any back reflections from the ring cavity. The ring contains a 2 GHz fiber-pigtailed lithium niobate electro-optic phase modulator (JDS Uniphase CATV dual output, x-cut) with an insertion loss of 4 dB and a V_π of ∼8.5 V. The modulator is driven by a sinusoidal radiofrequency (RF) signal source. By ensuring that the modulation frequency $\Omega/2\pi$ is much less than the FSR of the ring resonator, the effectively single-mode description of the system is valid. To overcome the insertion loss of the modulator and other components, we use a semiconductor optical amplifier (SOA). The SOA can operate with a maximum gain of 12 dB at 1542 nm; however, we operate it with a lower gain to compensate for intracavity losses without inducing lasing. With the intracavity loss compensated, the ring cavity has a finesse of up to 90 due to the input and output coupling. Lower finesse can be obtained by using a lower gain from the amplifier. The amplified spontaneous emission noise from the SOA was filtered using a dense-wavelength-division-multiplexing (DWDM) filter with a 3 dB bandwidth of 26 GHz and a center wavelength of 1542.14 nm. The bandpass filter also serves to inhibit spurious lasing near the peak gain wavelength of the SOA or other wavelengths where the fiber cavity round-trip loss is less than the loss at the input laser wavelength. Note that the bandwidth of this filter is much larger than the FSR of the ring resonator (4.1 or 15 MHz), so that its response is flat over the frequency range of interest here. A fiber polarization controller was used to align the input polarization to the principal axis of LiNbO$_3$ in the EOM. A drop port is incorporated using a second 99:1 fiber splitter. We exclusively use angle-polished fiber connectors (APC) throughout the setup to minimize back reflections and prevent exciting the countercirculating mode in the ring. The through-port and drop-port powers are monitored with InGaAs photodiodes with electrical bandwidths greater than 5 GHz. We also use a proportional-integral (PI) feedback loop (not shown in Figure 1) to lock the laser wavelength to a resonance of the ring cavity by actuating on the laser's frequency modulation input. Additionally, a fraction of the input laser light is frequency shifted using an acousto-optic modulator and then heterodyned with the cavity output if needed, to perform spectrally resolved field measurements (s_n) instead of power measurements ($|s_{1-}(t)|^2$ and $|s_{2-}(t)|^2$).

The adiabatic and nonadiabatic regimes can both be probed using this setup by appropriately choosing a combination of the modulation amplitude, the modulation frequency, and the optical amplifier gain to control A_0, Ω, and γ, respectively. For the adiabatic regime, we use a cavity with a line width of 200 kHz and a modulation frequency $\Omega/2\pi = 10$ kHz, which allows for a large modulation amplitude of $A_0/\Omega \leq 10$ while still satisfying eq 3. The nonadiabatic regime is explored using a
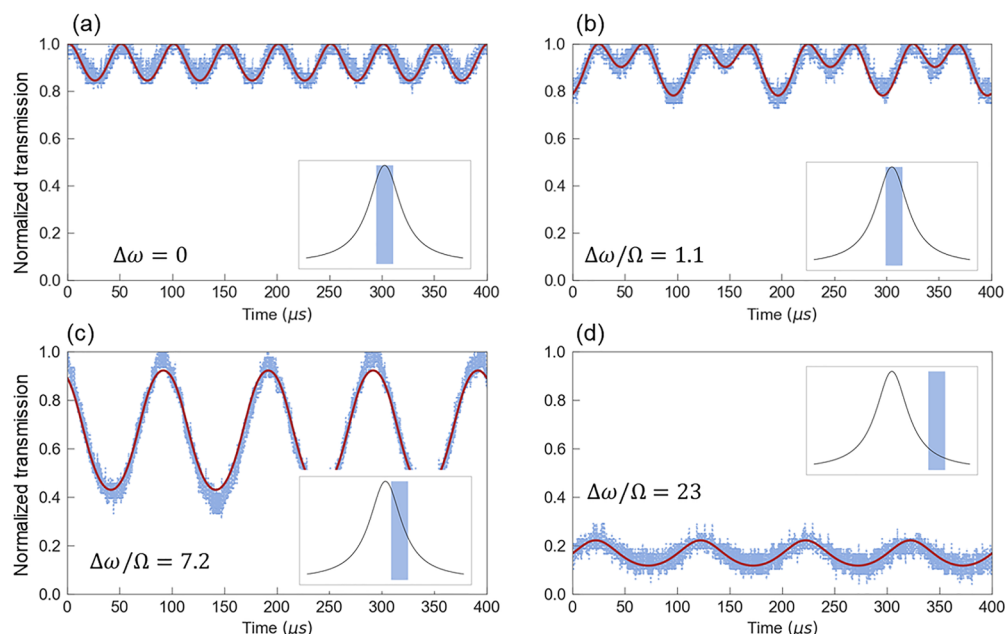
Figure 2. Normalized transmission through the cavity in the adiabatic regime recorded from the drop port, for various values of the input laser detuning $\Delta\omega/\Omega = 0$ (a), 1.1 (b), 7.2 (c), and 23 (d). The red solid lines are analytical curves based on eq 2 for the corresponding experimental data shown by blue dots. The insets in each figure show the static Lorentzian response of the cavity and the range over which the modulation sweeps the instantaneous resonance frequency. Here, the modulation frequency $\Omega = 2\pi \times 10$ kHz, much smaller than the line width $2\gamma = 2\pi \times 200$ kHz. Phase modulation amplitude $A_0/\Omega = 4.3$.

cavity with a similar line width of 270 kHz, but with a much larger modulation frequency of 1.3 MHz, enabling us to violate the adiabaticity condition in eq 3 with very small modulation amplitudes $A_0/\Omega \geq 0.01$.

RESULTS

Adiabatic Regime. We first study the cavity in the adiabatic regime that is typically associated with cavity EOMs and observe good agreement between the analytical predictions and experimental results, as depicted in Figure 2. For this regime, the cavity was implemented to have a line width $2\gamma = 2\pi \times 200$ kHz and an FSR of 4.1 MHz (finesse $\approx$ 20). The low finesse is beneficial for probing the adiabatic regime and was achieved by reducing the gain of the optical amplifier.

For a static cavity, the maximum transmission occurs for zero detuning and falls off with increasing values of detuning, as depicted by the insets in Figure 2. For the dynamically modulated cavity, we operate in the adiabatic regime by applying a modulation signal such that the peak phase excursion of the modulation is $A_0/\Omega = 4.3$, and $\Omega/2\pi = 10$ kHz. The adiabaticity condition (eq 3) is well satisfied by these parameters: $A_0/\Omega = 4.3 \ll (\gamma/\Omega)^2 = 100$. Here the slope of the static Lorentzian for a certain detuning determines the peak-to-peak swing of the transmission, as shown by the insets in Figure 2 and the corresponding transmission signals for various detunings (Figure 2(a)−(d)). These transmission signals were recorded from the drop port of the cavity. In this regime, the transmission varies as a function of time, and such a variation can be well understood using eq 2, where the transmitted power at any instant is determined by the instantaneous resonance frequency. At zero detuning (Figure 2a), the transmission varies at twice the frequency of the modulation due to the vanishing slope and the quadratic response near resonance. With larger detuning (Figure 2c and d), the

transmission varies at the frequencies of the modulation. The magnitude of the transmission variation decreases as the detuning increases. These behaviors are expected for a standard electro-optic cavity modulator.

Nonadiabatic, High-Frequency Regime. In contrast to the adiabatic regime presented above, we now experimentally observe the suppression of drop-port transmission and consequent dynamical input isolation in the nonadiabatic regime, as shown in Figure 3. For probing this regime, a shorter cavity was used ($2\gamma = 2\pi \times 270$ kHz, FSR = 15 MHz). A modulation frequency of $\Omega/2\pi = 1.3$ MHz ensured that the system operated in the high-frequency regime ($\Omega \gg \gamma$). In this
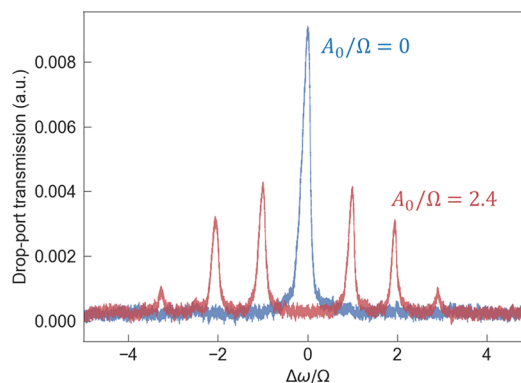

Figure 3. Nonadiabatic, high-frequency regime. Variation of the drop-port transmission with detuning for no modulation, $A_0/\Omega = 0$ (0 V_{pp}) and for $A_0/\Omega = 2.4$ ($\equiv 8.6$ V_{pp}), which is close to the zero of the Bessel function J_0. The transmission at zero detuning is suppressed by applying this modulation, resulting in dynamical input isolation. Cavity line width $2\gamma = 2\pi \times 270$ kHz, $\Omega = 2\pi \times 1.3$ MHz, FSR = 15 MHz. These parameter values satisfy both the constraints of single-mode operation ($\Omega/2\pi \ll$ FSR) and nonadiabatic high-frequency modulation ($\Omega \gg \gamma$, $A_0/\Omega \geq (\gamma/\Omega)^2 = 0.01$).

regime, nonadiabaticity is achieved even for a low modulation amplitude $A_0/\Omega > (\gamma/\Omega)^2 = 0.01$. To observe the transmission spectrum, we sweep the input laser frequency across a ring resonance slowly using a 200 Hz triangular ramp applied to fine-tune the input frequency and record the total transmitted power to measure the steady-state response of the modulated cavity at each input frequency. For $A_0/\Omega = 0$, the transmitted power exhibits a Lorentzian dependency with respect to the input frequency. On the other hand, when A_0/Ω is large, the transmitted power exhibits a peak whenever the input detuning is near $\Delta\omega = k\Omega$, as shown by the red curve in Figure 3, in agreement with eq 4. Moreover, when $A_0/\Omega \approx 2.4$, which approaches a zero of the Bessel function, as shown in Figure 3, the transmission nearly completely vanishes for an on-resonance input with $\Delta\omega = 0$. Such an absence of transmission signifies the effect of dynamic isolation: in the presence of modulation the cavity is no longer excited by an on-resonance input and hence is isolated from the input. As A_0/Ω varies from 0 to 2.4, the power transmission coefficient for an on-resonance input varies from 1 to 0. In this system, the amplitude of the sinusoidal modulation of the resonant frequency thus provides a switching mechanism based on the dynamical isolation effect.

More generally, we can suppress the transmission at a nonzero detuning that is an integer multiple of the modulation frequency, by choosing A_0/Ω to be a zero of the Bessel function of the appropriate order. One could also vary the modulation frequency to achieve a suppression of transmission at a desired detuning from the cavity in this manner. We illustrate this in Figure 4(a) by mapping out the drop-port transmission with detuning $\Delta\omega$ for increasing values of the modulation amplitude V_{pp}. A_0 in our experiments is determined by the peak-to-peak amplitude of the voltage applied to the EOM. Hence, to map out a larger range of A_0/Ω within the maximum achievable V_{pp} of 10 V, we use a lower modulation frequency $\Omega/2\pi = 0.8$ MHz. The drift in the spectrum between different modulation amplitudes was factored out. We see that with an increasing modulation amplitude, the transmission can be suppressed at $\Delta\omega/\Omega = 0$, ± 1 for $V_{pp} \approx 5.8, 9.3$, respectively, corresponding respectively to $A_0/\Omega = 2.4, 3.8$, which are close to the zeros of the Bessel function. The zero for $\Delta\omega/\Omega = \pm 2$ and higher orders is not attained due to the maximum achievable RF amplitude delivered by signal generator. Figure 4(b)−(d) show line cuts from Figure 4(a) for fixed detuning values corresponding to $\Delta\omega/\Omega = 0$ (blue), 1 (red), and 2 (green). The solid lines are fits based on the analytical prediction of eq 2 and show good agreement with the experimental data.

Lastly, we show a direct measurement of the output field by heterodyning the drop-port signal with a frequency-shifted version of the input laser, to recover the spectral components $s_n(\Delta\omega)$ in eq 1. For this experiment, about 90% of the input laser is split off and sent through a free-space acousto-optic modulator (AOM). The AOM is driven by an RF signal at 500 MHz, and the first-order diffraction from the AOM produces a beam that is up-shifted by 500 MHz in frequency. The output of the AOM is coupled back into the fiber and mixed with the drop-port signal at a 50:50 fiber beam splitter. The spectral components of this signal around 500 MHz yield the output field components $s_n(\Delta\omega)$. This process is repeated while scanning the input laser frequency, resulting in the plot in Figure 5. The experimental data agree very well with its analytically calculated counterpart based on eq 1 and outlined
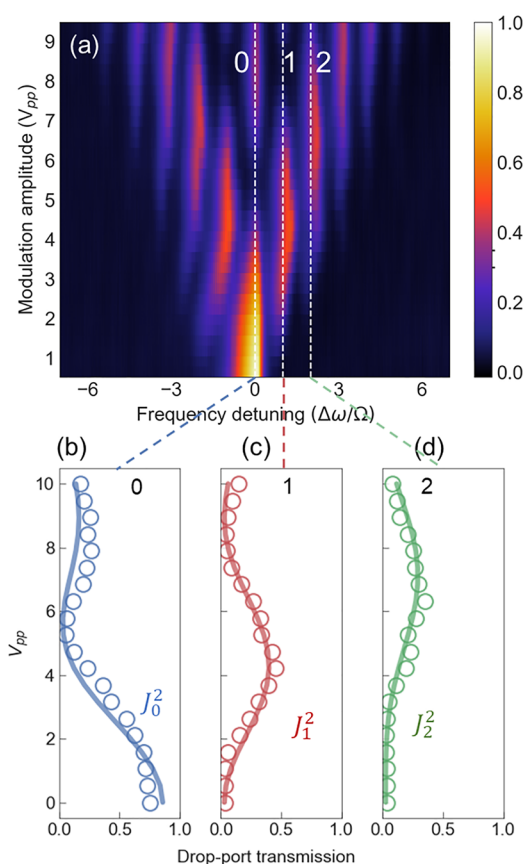

Figure 4. (a) Variation of the drop-port transmission with detuning and modulation amplitude. The drop-port transmission has been normalized to its maximum in the absence of modulation. (b)−(d) Line-outs along the dashed vertical lines in (a). The circles represent experimental data. The solid lines are fits to eq 1 for $\Delta\omega/\Omega = 0$, 1, and 2, which reduce to squares of the Bessel functions of the first kind and of the corresponding order. Zeroes of J_0 and J_1 are seen in the data. The drift in the spectrum on successive scans of increasing modulation amplitude was subtracted out.

in ref 33. For example, in Figure 5(a) and (b), $|s_{-1}|^2$ has peaks predominantly at $\Delta\omega/\Omega = 0$, 1, whereas $|s_2|^2$ has peaks at $\Delta\omega/\Omega = 0$, −1, −2. Figure 5(c) and (d) show the experimental and theoretical spectra for the case of dynamical isolation $A_0/\Omega = 2.4$. We see that s_n vanishes for all n at $\Delta\omega = 0$, as expected.

■ CONCLUSION AND FINAL REMARKS

We have experimentally demonstrated the theoretical predictions in the analytical work of Minkov et al.,[33] using a fiber ring resonator with an electro-optic phase modulator inside the cavity. We observed dynamical input isolation and suppression of drop-port transmission when the cavity was on resonance with the input laser, for appropriate parameters of the modulation. We also verified the behavior of this cavity in the adiabatic regime.

Similar demonstrations can be realized with on-chip photonic technologies, either by compensating the high insertion loss of chip-based EOMs with a gain medium inside the cavity or perhaps more practically by using low-loss EOMs such as those recently reported in lithium niobate.[51−57] For realizing gain on chip, several approaches exist, such as incorporating III−V-based amplifiers,[58−63] which requires electrical pumping, or using erbium doping or parametric
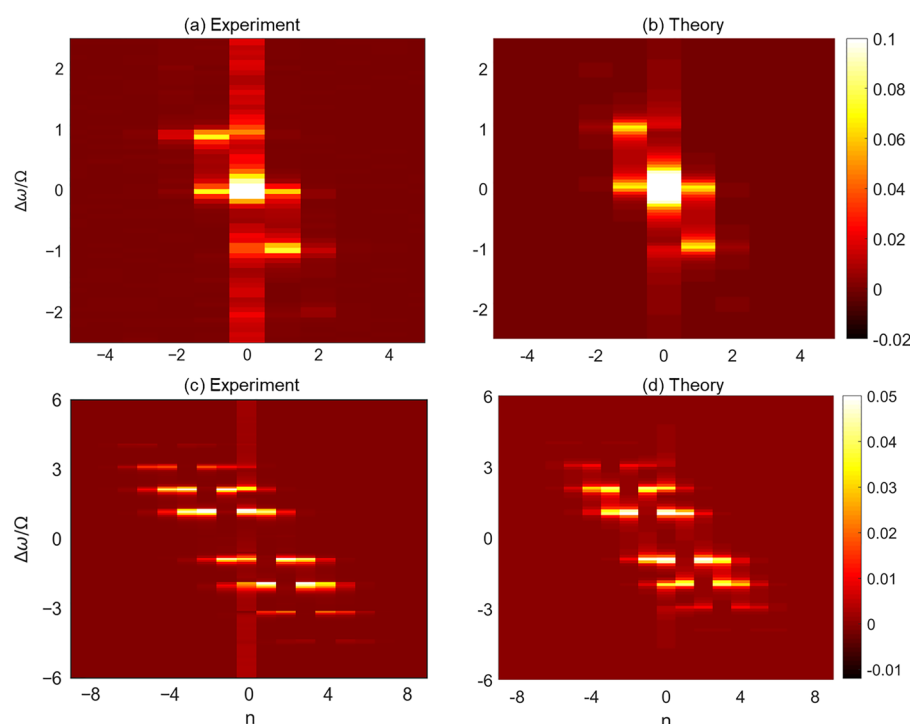
Figure 5. Spectral components $|s_n(\Delta\omega)|^2$ of the output field, measured experimentally using a heterodyne technique (a) and compared with the analytically calculated values (b) using eq 1. $A_0/\Omega = 0.6$, $\Omega/2\pi = 1$ MHz. (c and d) Same as (a) and (b) but under the criterion of dynamical isolation $A_0/\Omega = 2.4$, $\Omega/2\pi = 1.4$ MHz. $s_n(\Delta\omega = 0)$ vanishes in the case of dynamical isolation for all n. For all panels, $2\gamma = 2\pi \times 200$ kHz. Note the different x and y axis scales on the top and bottom panels.

gain, which require optical pumping.[64−71] The approach of utilizing on-chip gain might be especially important for implementing nonadiabatically modulated cavities in silicon. This is because silicon electro-optic modulators are based on the plasma dispersion effect, where an increasing modulation strength is inevitably concomitant with increasing loss.[72]

One could envision extending the current platform for frequency conversion and signal optimization by combining multiple harmonic modulations in tandem. Several theoretical proposals extend the dynamic modulation approach to an array of coupled cavities for realizing photonic gauge potentials, synthetic dimensions, and topological photonics and for controlling light transport,[23−26,28,46,73−78] and our experimental platform is ripe for realizing these proposals in an all-fiber configuration. Several of these applications would need to operate in a regime where the modulation frequency is commensurate with the FSR of the cavity, a regime that can readily be realized in our system. In a broader context of dynamical decoupling, the concept of modulating an open system at a rate faster than the time scale involved in the system−reservoir interaction has been proposed as a means of isolating it from the environment and suppressing decoherence.[35,36] This can be implemented and studied in a setup similar to the nonadiabatically modulated cavity we have presented, both for classical and for quantum optics applications.

AUTHOR INFORMATION

Corresponding Author

*E-mail: shanhui@stanford.edu.

ORCID

Avik Dutt: 0000-0002-6064-4356

Momchil Minkov: 0000-0003-0665-8412

Luqi Yuan: 0000-0001-9481-0247

REFERENCES

(1) Schmidt, B.; Xu, Q.; Shakya, J.; Manipatruni, S.; Lipson, M. Compact Electro-Optic Modulator on Silicon-on-Insulator Substrates Using Cavities with Ultra-Small Modal Volumes. *Opt. Express* **2007**, *15*, 3140−3148.

(2) Miller, D. A. B. Optical Interconnects to Silicon. *IEEE J. Sel. Top. Quantum Electron.* **2000**, *6*, 1312−1317.

(3) Taylor, H. F. Application of Guided-Wave Optics in Signal Processing and Sensing. *Proc. IEEE* **1987**, *75*, 1524−1535.

(4) Reed, G. T.; Mashanovich, G.; Gardes, F. Y.; Thomson, D. J. Silicon Optical Modulators. *Nat. Photonics* **2010**, *4*, 518−526.

(5) Tsang, M. Cavity Quantum Electro-Optics. *Phys. Rev. A: At., Mol., Opt. Phys.* **2010**, *81*, No. 063837.

(6) Tsang, M. Cavity Quantum Electro-Optics. II. Input-Output Relations between Traveling Optical and Microwave Fields. *Phys. Rev. A: At., Mol., Opt. Phys.* **2011**, *84*, No. 043845.

(7) Van, V.; Ibrahim, T. A.; Absil, P. P.; Johnson, F. G.; Grover, R.; Ho, P. T. Optical Signal Processing Using Nonlinear Semiconductor Microring Resonators. *IEEE J. Sel. Top. Quantum Electron.* **2002**, *8*, 705−713.

(8) Minasian, R. A. Photonic Signal Processing of Microwave Signals. *IEEE Trans. Microwave Theory Tech.* **2006**, *54*, 832−846.

(9) Creffield, C. E.; Sols, F. Directed Transport in Driven Optical Lattices by Gauge Generation. *Phys. Rev. A: At., Mol., Opt. Phys.* **2011**, *84*, No. 023630.

(10) Restrepo, S.; Cerrillo, J.; Bastidas, V. M.; Angelakis, D. G.; Brandes, T. Driven Open Quantum Systems and Floquet Stroboscopic Dynamics. *Phys. Rev. Lett.* **2016**, *117*, 250401.

(11) Dunlap, D. H.; Kenkre, V. M. Dynamic Localization of a Charged Particle Moving under the Influence of an Electric Field. *Phys. Rev. B: Condens. Matter Mater. Phys.* **1986**, *34*, 3625−3633.

(12) Eckardt, A.; Weiss, C.; Holthaus, M. Superfluid-Insulator Transition in a Periodically Driven Optical Lattice. *Phys. Rev. Lett.* **2005**, *95*, DOI: 10.1103/PhysRevLett.95.260404.

(13) Zenesini, A.; Lignier, H.; Ciampini, D.; Morsch, O.; Arimondo, E. Coherent Control of Dressed Matter Waves. *Phys. Rev. Lett.* **2009**, *102*, DOI: 10.1103/PhysRevLett.102.100403.

(14) Grossmann, F.; Dittrich, T.; Jung, P.; Hänggi, P. Coherent Destruction of Tunneling. *Phys. Rev. Lett.* **1991**, *67*, 516−519.

(15) Struck, J.; Ölschläger, C.; Weinberg, M.; Hauke, P.; Simonet, J.; Eckardt, A.; Lewenstein, M.; Sengstock, K.; Windpassinger, P. Tunable Gauge Potential for Neutral and Spinless Particles in Driven Optical Lattices. *Phys. Rev. Lett.* **2012**, *108*, 225304.

(16) Hauke, P.; Tieleman, O.; Celi, A.; Ölschläger, C.; Simonet, J.; Struck, J.; Weinberg, M.; Windpassinger, P.; Sengstock, K.; Lewenstein, M.; et al. Non-Abelian Gauge Fields and Topological Insulators in Shaken Optical Lattices. *Phys. Rev. Lett.* **2012**, *109*, 145301.

(17) Hargrove, L. E.; Fork, R. L.; Pollack, M. A. Locking of He−Ne Laser Modes Induced by Synchronous Intracavity Modulation. *Appl. Phys. Lett.* **1964**, *5*, 4−5.

(18) Ho, K. P.; Kahn, J. M. Optical Frequency Comb Generator Using Phase Modulation in Amplified Circulating Loop. *IEEE Photonics Technol. Lett.* **1993**, *5*, 721−725.

(19) Kourogi, M.; Enami, T.; Ohtsu, M. A Monolithic Optical Frequency Comb Generator. *IEEE Photonics Technol. Lett.* **1994**, *6*, 214−217.

(20) Diddams, S. A.; Ma, L.-S.; Ye, J.; Hall, J. L. Broadband Optical Frequency Comb Generation with a Phase-Modulated Parametric Oscillator. *Opt. Lett.* **1999**, *24*, 1747−1749.

(21) Shen, P.; Gomes, N. J.; Davies, P. A.; Huggard, P. G.; Ellison, B. N. Analysis and Demonstration of a Fast Tunable Fiber-Ring-Based Optical Frequency Comb Generator. *J. Lightwave Technol.* **2007**, *25*, 3257−3264.

(22) Ozharar, S.; Quinlan, F.; Ozdur, I.; Gee, S.; Delfyett, P. J. Ultraflat Optical Comb Generation by Phase-Only Modulation of Continuous-Wave Light. *IEEE Photonics Technol. Lett.* **2008**, *20*, 36−38.

(23) Yuan, L.; Shi, Y.; Fan, S. Photonic Gauge Potential in a System with a Synthetic Frequency Dimension. *Opt. Lett.* **2016**, *41*, 741−744.

(24) Lin, Q.; Xiao, M.; Yuan, L.; Fan, S. Photonic Weyl Point in a Two-Dimensional Resonator Lattice with a Synthetic Frequency Dimension. *Nat. Commun.* **2016**, *7*, 13731.

(25) Ozawa, T.; Price, H. M.; Goldman, N.; Zilberberg, O.; Carusotto, I. Synthetic Dimensions in Integrated Photonics: From Optical Isolation to Four-Dimensional Quantum Hall Physics. *Phys. Rev. A: At., Mol., Opt. Phys.* **2016**, *93*, No. 043827.

(26) Hey, D.; Li, E. Advances in Synthetic Gauge Fields for Light through Dynamic Modulation. *R. Soc. Open Sci.* **2018**, *5*, 172447.

(27) Yuan, L.; Fan, S. Bloch Oscillation and Unidirectional Translation of Frequency in a Dynamically Modulated Ring Resonator. *Optica* **2016**, *3*, 1014−1018.

(28) Yuan, L.; Xiao, M.; Lin, Q.; Fan, S. Synthetic Space with Arbitrary Dimensions in a Few Rings Undergoing Dynamic Modulation. *Phys. Rev. B: Condens. Matter Mater. Phys.* **2018**, *97*, 104105.

(29) Lin, H.; Ogbuu, O.; Liu, J.; Zhang, L.; Michel, J.; Hu, J. Breaking the Energy-Bandwidth Limit of Electrooptic Modulators: Theory and a Device Proposal. *J. Lightwave Technol.* **2013**, *31*, 4029−4036.

(30) Gardes, F. Y.; Brimont, A.; Sanchis, P.; Rasigade, G.; Marris-Morini, D.; O'Faolain, L.; Dong, F.; Fedeli, J. M.; Dumon, P.; Vivien, L.; et al. High-Speed Modulation of a Compact Silicon Ring Resonator Based on a Reverse-Biased Pn Diode. *Opt. Express* **2009**, *17*, 21986−21991.

(31) Sacher, W. D.; Poon, J. K. S. Dynamics of Microring Resonator Modulators. *Opt. Express* **2008**, *16*, 15741−15753.

(32) Timurdogan, E.; Sorace-Agaskar, C. M.; Sun, J.; Hosseini, E. S.; Biberman, A.; Watts, M. R. An Ultralow Power Athermal Silicon Modulator. *Nat. Commun.* **2014**, *5*, 4008.

(33) Minkov, M.; Shi, Y.; Fan, S. Exact Solution to the Steady-State Dynamics of a Periodically Modulated Resonator. *APL Photonics* **2017**, *2*, No. 076101.

(34) Salerno, G.; Carusotto, I. Dynamical Decoupling and Dynamical Isolation in Temporally Modulated Coupled Pendulums. *Europhys. Lett.* **2014**, *106*, 24002.

(35) Viola, L.; Knill, E.; Lloyd, S. Dynamical Decoupling of Open Quantum Systems. *Phys. Rev. Lett.* **1999**, *82*, 2417−2421.

(36) Viola, L.; Lloyd, S. Dynamical Suppression of Decoherence in Two-State Quantum Systems. *Phys. Rev. A: At., Mol., Opt. Phys.* **1998**, *58*, 2733−2744.

(37) Holthaus, M.; Hone, D. Quantum Wells and Superlattices in Strong Time-Dependent Fields. *Phys. Rev. B: Condens. Matter Mater. Phys.* **1993**, *47*, 6499−6508.

(38) Yang, W.; Wang, Z.-Y.; Liu, R.-B. Preserving Qubit Coherence by Dynamical Decoupling. *Front. Phys.* **2011**, *6*, 2−14.

(39) Mortezapour, A.; Franco, R. L. Protecting Quantum Resources via Frequency Modulation of Qubits in Leaky Cavities. *Sci. Rep.* **2018**, *8*, 14304.

(40) Alaeian, H.; Chang, C. W. S.; Moghaddam, M. V.; Wilson, C. M.; Solano, E.; Rico, E. Lattice Gauge Fields via Modulation in Circuit QED: The Bosonic Creutz Ladder. *arXiv:1805.12410*, 2018.

(41) Wilson, C. M.; Duty, T.; Sandberg, M.; Persson, F.; Shumeiko, V.; Delsing, P. Photon Generation in an Electromagnetic Cavity with a Time-Dependent Boundary. *Phys. Rev. Lett.* **2010**, *105*, 233907.

(42) Haus, H. A. *Waves and Fields in Optoelectronics*; Prentice Hall: Englewood Cliffs, NJ, 1984.

(43) Little, B. E.; Chu, S. T.; Haus, H. A.; Foresi, J. Microring Resonator Channel Dropping Filters. *J. Lightwave Technol.* **1997**, *15*, 998−1005.

(44) Yu, H.; Ying, D.; Pantouvaki, M.; Campenhout, J. V.; Absil, P.; Hao, Y.; Yang, J.; Jiang, X. Trade-off between Optical Modulation Amplitude and Modulation Bandwidth of Silicon Micro-Ring Modulators. *Opt. Express* **2014**, *22*, 15178−15189.

(45) Ehrlichman, Y.; Khilo, A.; Popović, M. A. Optimal Design of a Microring Cavity Optical Modulator for Efficient RF-to-Optical Conversion. *Opt. Express* **2018**, *26*, 2462−2477.

(46) Minkov, M.; Fan, S. Localization and Time-Reversal of Light through Dynamic Modulation. *Phys. Rev. B: Condens. Matter Mater. Phys.* **2018**, *97*, No. 060301.

(47) Okamura, H.; Iwatsuki, K. A Finesse-Enhanced Er-Doped-Fiber Ring Resonator. *J. Lightwave Technol.* **1991**, *9*, 1554−1560.

(48) Vatnik, I. D.; Tikan, A.; Onishchukov, G.; Churkin, D. V.; Sukhorukov, A. A. Anderson Localization in Synthetic Photonic Lattices. *Sci. Rep.* **2017**, *7*, 4301.

(49) McMahon, P. L.; Marandi, A.; Haribara, Y.; Hamerly, R.; Langrock, C.; Tamate, S.; Inagaki, T.; Takesue, H.; Utsunomiya, S.; Aihara, K.; et al. A Fully Programmable 100-Spin Coherent Ising Machine with All-to-All Connections. *Science* **2016**, *354*, 614−617.

(50) Kaiser, F.; Fedrici, B.; Zavatta, A.; D'Auria, V.; Tanzilli, S. A Fully Guided-Wave Squeezing Experiment for Fiber Quantum Networks. *Optica* **2016**, *3*, 362−365.

(51) Wang, C.; Burek, M. J.; Lin, Z.; Atikian, H. A.; Venkataraman, V.; Huang, I.-C.; Stark, P.; Lončar, M. Integrated High Quality Factor Lithium Niobate Microdisk Resonators. *Opt. Express* **2014**, *22*, 30924−30933.

(52) Wang, C.; Zhang, M.; Stern, B.; Lipson, M.; Lončar, M. Nanophotonic Lithium Niobate Electro-Optic Modulators. *Opt. Express* **2018**, *26*, 1547−1555.

(53) Zhang, M.; Wang, C.; Cheng, R.; Shams-Ansari, A.; Lončar, M. Monolithic Ultra-High-Q Lithium Niobate Microring Resonator. *Optica* **2017**, *4*, 1536−1537.

(54) Jiang, W. C.; Lin, Q. Chip-Scale Cavity Optomechanics in Lithium Niobate. *Sci. Rep.* **2016**, *6*, 36920.

(55) Krasnokutska, I.; Tambasco, J.-L. J.; Li, X.; Peruzzo, A. Ultra-Low Loss Photonic Circuits in Lithium Niobate on Insulator. *Opt. Express* **2018**, *26*, 897−904.

(56) Witmer, J. D.; Valery, J. A.; Arrangoiz-Arriola, P.; Sarabalis, C. J.; Hill, J. T.; Safavi-Naeini, A. H. High-Q Photonic Resonators and Electro-Optic Coupling Using Silicon-on-Lithium-Niobate. *Sci. Rep.* **2017**, *7*, 46313.

(57) Boes, A.; Corcoran, B.; Chang, L.; Bowers, J.; Mitchell, A. Status and Potential of Lithium Niobate on Insulator (LNOI) for Photonic Integrated Circuits. *Laser Photonics Rev.* **2018**, *12*, 1700256.

(58) Park, H.; Fang, A. W.; Kodama, S.; Bowers, J. E. Hybrid Silicon Evanescent Laser Fabricated with a Silicon Waveguide and III-V Offset Quantum Wells. *Opt. Express* **2005**, *13*, 9460−9464.

(59) Guan, H.; Novack, A.; Galfsky, T.; Ma, Y.; Fathololoumi, S.; Horth, A.; Huynh, T. N.; Roman, J.; Shi, R.; Caverley, M.; et al. Widely-Tunable, Narrow-Linewidth III-V/Silicon Hybrid External-Cavity Laser for Coherent Communication. *Opt. Express* **2018**, *26*, 7920−7933.

(60) Keyvaninia, S.; Roelkens, G.; Thourhout, D. V.; Jany, C.; Lamponi, M.; Liepvre, A. L.; Lelarge, F.; Make, D.; Duan, G.-H.; Bordel, D.; et al. Demonstration of a Heterogeneously Integrated III-V/SOI Single Wavelength Tunable Laser. *Opt. Express* **2013**, *21*, 3784−3792.

(61) Stern, B.; Ji, X.; Dutt, A.; Lipson, M. Compact Narrow-Linewidth Integrated Laser Based on a Low-Loss Silicon Nitride Ring Resonator. *Opt. Lett.* **2017**, *42*, 4541−4544.

(62) Zhang, J.; Li, Y.; Dhoore, S.; Morthier, G.; Roelkens, G. Unidirectional, Widely-Tunable and Narrow-Linewidth Heterogeneously Integrated III-V-on-Silicon Laser. *Opt. Express* **2017**, *25*, 7092−7100.

(63) Mechet, P.; Verstuyft, S.; de Vries, T.; Spuesens, T.; Regreny, P.; Thourhout, D. V.; Roelkens, G.; Morthier, G. Unidirectional III-V Microdisk Lasers Heterogeneously Integrated on SOI. *Opt. Express* **2013**, *21*, 19339−19352.

(64) Belt, M.; Blumenthal, D. J. Erbium-Doped Waveguide DBR and DFB Laser Arrays Integrated within an Ultra-Low-Loss Si_3N_4 Platform. *Opt. Express* **2014**, *22*, 10655−10660.

(65) Han, H.-S.; Seo, S.-Y.; Shin, J. H. Optical Gain at 1.54 μm in Erbium-Doped Silicon Nanocluster Sensitized Waveguide. *Appl. Phys. Lett.* **2001**, *79*, 4568−4570.

(66) Kik, P. G.; Polman, A. Erbium-Doped Optical-Waveguide Amplifiers on Silicon. *MRS Bull.* **1998**, *23*, 48−54.

(67) Purnawirman; Sun, J.; Adam, T. N.; Leake, G.; Coolbaugh, D.; Bradley, J. D. B.; Hosseini, E. S.; Watts, M. R. C- and L-Band Erbium-Doped Waveguide Lasers with Wafer-Scale Silicon Nitride Cavities. *Opt. Lett.* **2013**, *38*, 1760−1762.

(68) Grivas, C. Optically Pumped Planar Waveguide Lasers: Part II: Gain Media, Laser Systems, and Applications. *Prog. Quantum Electron.* **2016**, *45−46*, 3−160.

(69) Pollnau, M. Rare-Earth-Ion-Doped Channel Waveguide Lasers on Silicon. *IEEE J. Sel. Top. Quantum Electron.* **2015**, *21*, 414−425.

(70) Hosseini, E. S.; Purnawirman; Bradley, J. D. B.; Sun, J.; Leake, G.; Adam, T. N.; Coolbaugh, D. D.; Watts, M. R. CMOS-Compatible 75 MW Erbium-Doped Distributed Feedback Laser. *Opt. Lett.* **2014**, *39*, 3106−3109.

(71) Foster, M. A.; Turner, A. C.; Sharping, J. E.; Schmidt, B. S.; Lipson, M.; Gaeta, A. L. Broad-Band Optical Parametric Gain on a Silicon Photonic Chip. *Nature* **2006**, *441*, 960−963.

(72) Soref, R.; Bennett, B. Electrooptical Effects in Silicon. *IEEE J. Quantum Electron.* **1987**, *23*, 123−129.

(73) Yuan, L.; Xiao, M.; Fan, S. Time Reversal of a Wave Packet with Temporal Modulation of Gauge Potential. *Phys. Rev. B: Condens. Matter Mater. Phys.* **2016**, *94*, DOI: 10.1103/PhysRevB.94.140303.

(74) Yanik, M. F.; Fan, S. Time Reversal of Light with Linear Optics and Modulators. *Phys. Rev. Lett.* **2004**, *93*, 173903.

(75) Qin, C.; Zhou, F.; Peng, Y.; Sounas, D.; Zhu, X.; Wang, B.; Dong, J.; Zhang, X.; Alù, A.; Lu, P. Spectrum Control through Discrete Frequency Diffraction in the Presence of Photonic Gauge Potentials. *Phys. Rev. Lett.* **2018**, *120*, 133901.

(76) Bell, B. A.; Wang, K.; Solntsev, A. S.; Neshev, D. N.; Sukhorukov, A. A.; Eggleton, B. J. Spectral Photonic Lattices with Complex Long-Range Coupling. *Optica* **2017**, *4*, 1433−1436.

(77) Minkov, M.; Savona, V. Haldane Quantum Hall Effect for Light in a Dynamically Modulated Array of Resonators. *Optica* **2016**, *3*, 200.

(78) Salerno, G.; Ozawa, T.; Price, H. M.; Carusotto, I. Floquet Topological System Based on Frequency-Modulated Classical Coupled Harmonic Oscillators. *Phys. Rev. B: Condens. Matter Mater. Phys.* **2016**, *93*, No. 085105.